Ocean Dynamics (2025) 75:20
https://doi.org/10.1007/s10236-025-01668-5

The reflux of water transport in the intermediate layer of Luzon Strait

Ziyun Yang[1] · Wei Zhuang[1] · Hongyang Lin[1,2] · Jianyu Hu[1,2,3]

Received: 2 October 2024 / Accepted: 10 February 2025
© Springer-Verlag GmbH Germany, part of Springer Nature 2025

Abstract
Based on Lagrangian particle tracking experiments using long-term, high-resolution reanalysis data, we investigate the pathways of water transport and reflux at different depths in the intermediate layer of the Luzon Strait (LS). Reflux is defined as the phenomenon where particles, once released at the 121°E section, subsequently return to the same section. The results indicate that the majority of reflux occurs within 60 days and can be categorized into two scenarios according to the return time. The case with the shorter return time involves higher-frequency flow variations in the LS. In contrast, the case with the longer return time not only modifies the zonal transport across the LS but also facilitates meridional connections between the northern outflow toward the western Pacific Ocean and the central inflow into the South China Sea (SCS). The pattern and seasonal variations of reflux vary significantly with depth. At the 500 m depth, the reflux is mainly attributed to the central inflow associated with the Kuroshio intrusion, with only 5% of the northern outflow returning to the 121°E section. At the 1250 m layer, the northern outflow is more prone to reflux, with 60% flowing back to the section, while the reflux of central inflow results in only a small fraction of the inflow water returning to the western Pacific Ocean. These findings highlight the critical role of reflux processes in regulating intermediate-layer water exchanges through the LS, contributing to a more comprehensive understanding of the interactions between the western Pacific and the SCS.

Keywords Luzon Strait · Lagrangian particle tracking · Intermediate layer transport · Reflux

1 Introduction

The South China Sea (SCS) is the largest tropical marginal sea in the western Pacific Ocean, covering an area of about 3.5 million square kilometers. The maximum water depth in the SCS exceeds 5,000 m, with several straits and channels connecting it to adjacent waters, e.g. the western Pacific Ocean, East China Sea, Java Sea, and Sulu Sea. The Luzon Strait (LS) is the only deep-water passage facilitating exchange between the SCS and the western Pacific Ocean at intermediate and deep layers (Fig. 1). Consequently, the SCS exhibits a semi-enclosed structure in these layers (Qu et al. 2006), and the transport in the LS is closely related to the ocean processes in both the SCS and the western Pacific. The LS stands out as the most significant, intense, and complex water exchange pathway among all the straits in the SCS. Observations show that the water transport in the LS has a vertically-stratified sandwiched structure (Tian et al. 2006; Yuan et al. 2008). This structure not only regulates the horizontal circulation and the material and energy transports in the SCS (Gan et al. 2006, 2016; Hu et al. 2012; Lan et al. 2013, 2015; Nan et al. 2015; Cai et al. 2020) but also controls the SCS meridional overturning circulation and the vertical cross-layer transport (Shu et al. 2014; Wang et al. 2016; Zhu et al. 2016).

In terms of the vertical sandwiched structure of the LS transport, there is an overall inflow from the western Pacific Ocean to the SCS in the upper layer (<500 m) of the LS, with a seasonal variation characterized by a stronger inflow in winter and a weaker inflow in summer (Sun et al. 2023). Previous research indicated that the upper-layer transport is significantly related to the Kuroshio intensity as well as its

Responsible Editor: Yasumasa Miyazawa.

✉ Wei Zhuang
wzhuang@xmu.edu.cn

[1] State Key Laboratory of Marine Environmental Science, College of Ocean and Earth Sciences, Xiamen University, Xiamen 361102, China

[2] Southern Marine Science and Engineering Guangdong Laboratory (Zhuhai), Zhuhai 519082, China

[3] Center for Marine Meteorology and Climate Change, Xiamen University, Xiamen 361102, China

Published online: 19 February 2025

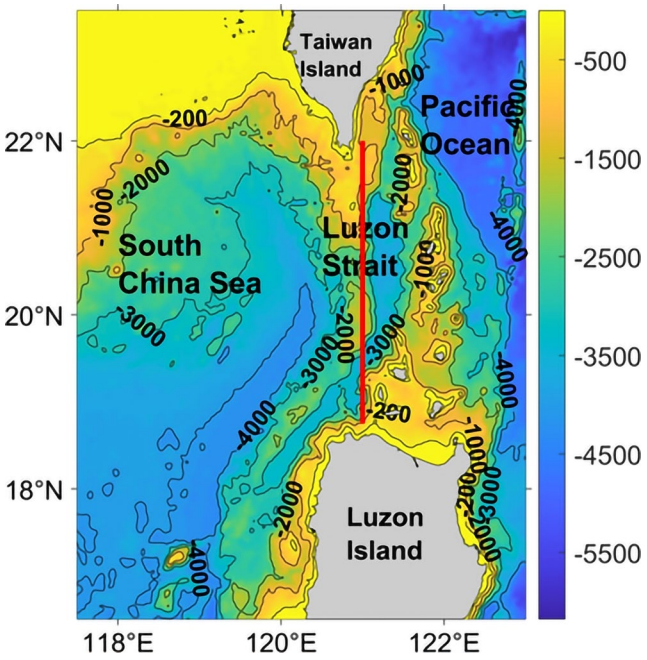

Fig. 1 Topography of the LS and its surrounding areas (the unit of bathymetric contour is meter). The red solid line represents the 121°E section

intrusion pattern into the SCS (Chen et al. 2011). Moreover, the LS roughly lies in the band of subtropical countercurrent which possesses the second most intense eddy activity in the North Pacific (Aoki and Imawaki 1996). Although a majority of the westward-propagating mesoscale eddies dissipate in the western boundary layer (Zhai et al. 2010), there are abundant evidence of mesoscale eddies propagating from the Pacific Ocean to the SCS via the LS (Zheng et al. 2008; Hu et al. 2012), which leads to significant eddy activity in the upper layer of the LS (Li et al. 1998; Trott et al. 2021).

The intermediate layer of the LS, ranging approximately from 500 m to 1200 m in depth, is characterized by a net outflow of about 2.4 Sv from the SCS to the Pacific Ocean (Yuan et al. 2009). Within this depth range, the vertical mixing can reach to the order value of 10^{-2} m^2 s^{-1}, which is much stronger than that in the open ocean (Tian et al. 2009). The full-depth hydrographic observations indicate that the outflow in the intermediate layer of the LS is controlled by advection and mixing (Shen et al. 2022). Tian et al. (2006) suggested that this intermediate outflow is not spatially uniform, featuring an eastward outflow north of 20°N and a westward inflow south of 20°N. Subsequently Xie et al. (2011), based on the same measurements of Tian et al. (2006), indicated that such a flow pattern corresponds to a subsurface anticyclonic eddy in the LS; they further pointed out that the anticyclonic eddy significantly reduces the intermediate water exchange between the SCS and the western Pacific Ocean by recirculating a substantial portion of the eastward transport back into the SCS. The existence of an intermediate-layer anticyclonic eddy in the LS has also been confirmed through the water isotope analysis (Wu et al. 2021), suggesting that the eddy activity occurs not only at the surface of the LS but also within its intermediate layer. The problem is that existing studies on the intermediate layer transport are based on short-term observations, which do not allow for detailed investigations on the amount of water recirculation and its seasonal variations affected by the eddy. Moreover, most previous studies concentrated on the net transport changes of the entire intermediate layer, but ignored its detailed vertical structures that may affect the water exchange.

Therefore, this study aims to explore detailed features of water transport in the intermediate layer of the LS based on long-term, high-resolution reanalysis data and the Lagrangian particle tracking method. In this study, we focus on the pattern, quantity, and seasonal variations of the intermediate layer transport and reflux in the LS. The rest of this paper is organized as follows. Section 2 introduces the reanalysis data used in the study and the particle tracking method. Section 3 presents the flow field in the LS and the transport at different depths. Section 4 discusses the seasonal and interannual variations of reflux, and Sect. 5 summarizes the main results and provides prospects for future research.

2 Data and methods

2.1 Reanalysis data

This study uses the HYCOM (HYbrid Coordinate Ocean Model)+NCODA (Navy Coupled Ocean Data Assimilation) GOFS 3.1 (Global Ocean Forecasting System 3.1) global reanalysis data (https://www.hycom.org/dataserver/gofs-3pt1/reanalysis) on the GLBv0.08 grid. The model spans from 40°S to 40°N with a horizontal resolution of 0.08°×0.08°, and vertically has 41 layers with a resolution of 10–100 m in the upper 500 m and 100–1000 m in the intermediate and deep layers. The HYCOM model is driven by CFSR (1-hourly National Centers for Environmental Prediction Climate Forecast System Reanalysis) and CFSv2 (Climate Forecast System Version 2) as the surface forcing, and is assimilated with the NCODA data (Navy Coupled Ocean Data Assimilation; Cummings and Smedstad 2013) which integrate satellite data and in-situ observations. Previous studies have demonstrated that this reanalysis dataset is generally able to reproduce numerous oceanic processes in different layers of the LS and the SCS (Xie et al. 2011; Zhang et al. 2013; Lan et al. 2015; Jiang et al. 2020; Sun et al. 2023). Compared to GOFS3.0, GOFS3.1 has improved the vertical resolution of the surface ocean,

refined the surface atmospheric forcing formula, the internal simulation formula, and hence has a better simulation performance. The selected study area is the LS region (118°-123°E, 17°-23°N), covering 22 years from 1994 to 2015 with daily-averaged data. The relatively long-term coverage of the reanalysis enables us to obtain more accurate climatological fields. In addition, the LS transport patterns and the associated seasonal variations obtained from this HYCOM reanalysis (Fig. 2a-d) also agree well with the observations (Fig. 2e-h; from Fig. 8 of Zhang et al. 2015).

2.2 Lagrangian particle tracking

In this study, the Parcels toolkit is employed for performing Lagrangian particle tracking in the study area. Compared to other toolkits, Parcels toolkit demonstrates evident advantages such as its rapid execution and easy extensibility (Lange and Sebille 2017; Kehl et al. 2023). The calculation of Lagrangian particle trajectories is as follows:

$$\boldsymbol{X}\left(t+\delta\, t\right)=\boldsymbol{X}\left(t\right)+\int_{t}^{t+\delta\, t}\boldsymbol{v}\left(\boldsymbol{x},\tau\,\right)d\tau$$

where $\boldsymbol{X}$ denotes the centroid position of the particles, t represents time, δt signifies the time interval, and $\boldsymbol{v}(\boldsymbol{x},\tau)$ denotes the HYCOM flow field corresponding to the particle's location. The fourth-order Runge–Kutta method for explicit time operations, with a time step of 12 h, has been applied to solve the equation. Particles are released at the 121°E section (see Fig. 1 for the location) with a spatial interval of 0.06° and a temporal interval of 1 day. We employ a sliding boundary condition to ensure that the movement of particles is not impeded by the shoreline. The particle release timeframe spans from 1994 to 2014, and their movement is calculated from 1994 to 2015, so the majority of particles can exit the domain within this period. The transport represented by the particles is calculated as follows:

$$\boldsymbol{Tr}\left(\boldsymbol{x},t\right)=\boldsymbol{v}\left(\boldsymbol{x},t\right)*L\left(\boldsymbol{x}\right)$$

where $\boldsymbol{Tr}$ represents the water transport of the particle, and L denotes the spatial interval between particles. This formula implies that particles with higher release velocities represent larger water transport, under the assumption that the water volume represented by each particle remains constant throughout its trajectory.

It is noteworthy that the HYCOM reanalysis product provides both 3-hour and daily outputs. To examine the sensitivity of particle trajectories to the temporal resolution of flow fields, we conducted three Lagrangian particle tracking experiments using 3-hour, daily, and weekly mean flow fields, respectively. The results of these sensitive runs show that the trajectories of water particles estimated from 3-hour and daily ocean flows exhibit little discrepancies, while those based on weekly mean flow fields differ significantly, likely due to the loss of high-frequency flow variability (figures not shown). Therefore, this study adopts the daily HYCOM output to further calculate the details of particle trajectories around the Luzon Strait.

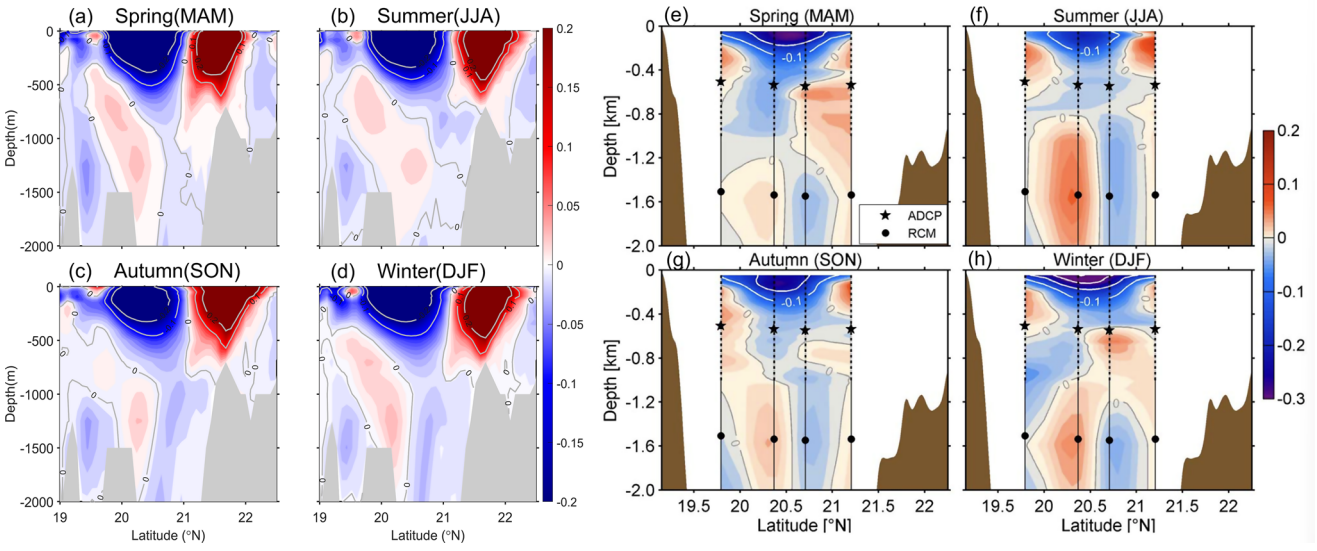

Fig. 2 Seasonal pattern of zonal flows (in m s^{-1}) across the 121°E section in the LS obtained from the HYCOM reanalysis. (**a**) spring, (**b**) summer, (**c**) autumn, and (**d**) winter. The flows are averaged from April 2012 to March 2013, the same period as the observasional results (**e**-**h**) cited from Figure 8 of Zhang et al. (2015)

3 Results

3.1 Seasonal variations of flow pattern at the Luzon Strait

The 121°E section of the LS, situated between the Luzon Island and the Taiwan Island (see Fig. 1), is selected to calculate water volume transport within the LS. Observations reveal a distinct sandwich-like vertical structure of water volume transport through the LS, characterized by westward—eastward—westward flows pattern from the surface to deep layers (Tian et al. 2006). This pattern is reproduced by our results calculated using HYCOM reanalysis data (Fig. 3a). Hereinafter, we define the westward flow into the SCS as inflow, and the eastward flow to the western Pacific Ocean as outflow. To determine the depth of different layers, we linearly interpolate the zonal flow into 1-m intervals and thus partition the water column of the LS into upper, intermediate, and deep layers according to the zonal transport direction. The upper layer (0–412 m) exhibits higher inflow velocities and the largest transport. The annual mean zonal velocity first decreases from the surface to 50 m depth, then increases from 50 m to 125 m, and decreases from 125 m to 412 m. Moreover, this layer exhibits pronounced seasonal variability with a stronger inflow in winter and an outflow in summer. The intermediate layer (412–1252 m) corresponds to an eastward outflow transport in the LS, with significantly lower magnitudes of both velocity and transport compared to their upper-layer counterparts; the intermediate-layer flow also has a clear seasonality with relatively enhanced outflow in winter while weakened one in summer. The deep layer primarily features a westward transport, and its seasonal changes differ from the upper and intermediate layers with a stronger inflow in summer while a weaker one in winter.

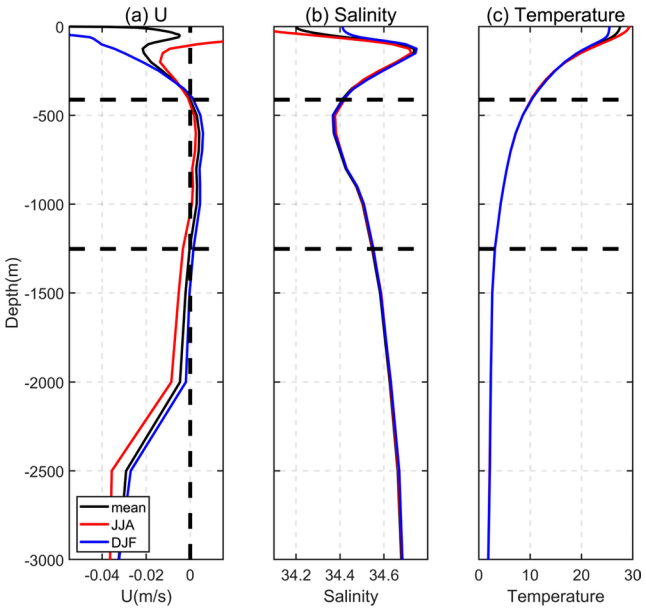

Fig. 3 The vertical profile of the mean (**a**) zonal velocity U, (**b**) salinity, and (**c**) temperature at the 121ºE transect in the LS. The black line represents the mean state, the red and blue lines indicate the climatological state for summer and winter, respectively. Two horizontal dashed lines indicate the depths of 412 m and 1252 m, respectively

Seasonal variations of temperature and salinity in the LS are predominantly confined to the upper layer with lower temperature and higher salinity in winter and higher temperature and lower salinity in summer (Fig. 3b, c). This layer includes both the surface low-salinity water and the subsurface high-salinity water (Fig. 3b), corresponding to the mixed layer and the main body of the thermocline (Fig. 3c). The intermediate layer is characterized by the intermediate low-salinity water, while the deep layer features high-salinity and low-temperature water. There is no obvious seasonal variation in temperature and salinity in the intermediate and deep layers.

The annual mean current on the 121°E section of the LS is predominantly eastward north of 21°N but westward south of 21°N (Fig. 4a). The maximum eastward and westward velocities occur near 21.8°N and 20.2°N, respectively, with the eastward flow exceeding the westward flow by about 0.2 m/s. This current pattern is consistent with the Kuroshio intrusion pattern with northwestward (eastward) flowing in the central (northern) part of LS. Along the main axis of the westward inflow, the velocity decreases with depth, reaching approximately 0 m/s around 1252 m, below which the deep-layer current is primarily westward.

The current field in the LS also exhibits pronounced seasonal variations. The wintertime westward flow in the central part of LS is clearly stronger than its summertime counterpart throughout the upper layer, as expected given the enhanced intrusion of the Kuroshio in winter (Fig. 4b). In summer, the weakened Kuroshio intrusion is not only associated with a weaker westward flow in the central part but also with a stronger eastward flow in the northern part of LS (Fig. 4c), which leads to the total upper-layer transport transitioning from an inflow in winter to an outflow in summer. The eastward flow at 21.8°N intensifies from 0.2 m/s in winter to 0.4 m/s in summer. In the intermediate and deep layers, the wintertime current field generally shows an enhanced outflow, while the summertime current is marked by an increased inflow. The intermediate layer is similar to upper layer that features outflow in the northern part and inflow in the central part. Closer inspection suggests that the flow pattern is almost unchanged in the upper intermediate layer, but in the lower intermediate layer (1000–1252 m depth), the flow direction between 20.4° and 21°N (the black box in Fig. 4) changes from an outflow in winter to an inflow in summer. That means the seasonal variation in zonal flow direction opposes to each other in

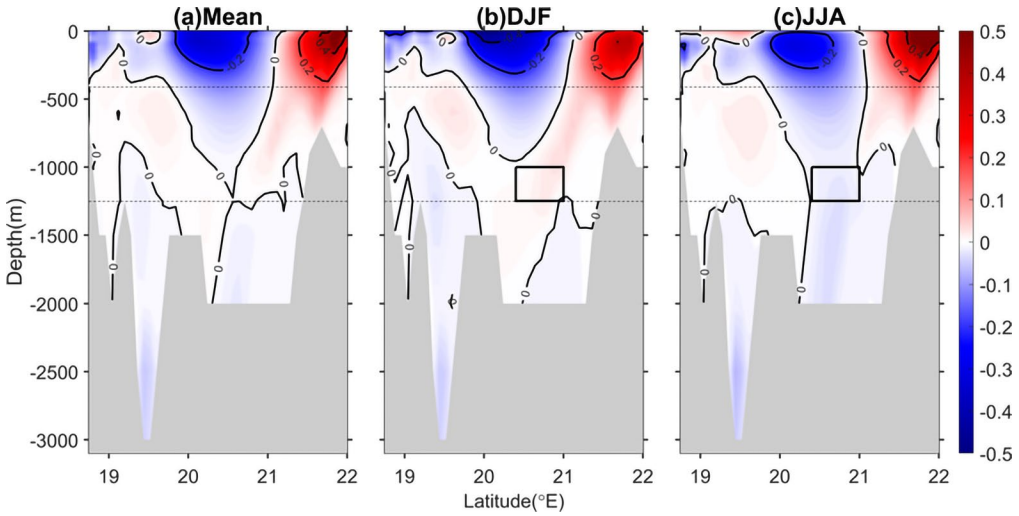

Fig. 4 The zonal velocity of (**a**) annual mean, (**b**) winter mean and (**c**) summer mean at the 121°E transect in the LS. Positive eastwards, and the magnitude is m/s. The black box indicates the region where flow direction changes in the lower intermediate layer

the upper and lower intermediate layers, and should be discussed separately.

3.2 Meridional and seasonal variations of intermediate-layer transport in the Luzon Strait

Given the distinct flow patterns in the LS mentioned above, we now further examined the meridional distribution of the intermediate-layer (412–1252 m) zonal transport along the 121°E section and its seasonal variations (Fig. 5a). The section can be meridionally divided into three segments according to the mean transport estimated from HYCOM output: the northern outflow (from 20.8°N to 22°N), the central inflow (from 19.8°N to 20.8°N), and the southern outflow (south of 19.8°N). The maximum eastward outflow in the northern segment is located near 21.6°N, and the maximum westward inflow in the central segment is near 20.5°N. Collectively, the entire section shows an overall eastward outflow in the intermediate layer, with a stronger transport in winter than that in summer. Among these segments, the northern outflow and the central westward inflow exhibits larger magnitudes of zonal transports and clearer seasonal variations (Fig. 5b). In winter, the northern eastward flow induces a total outflow transport of approximately 2.4 Sv, covering a relatively large meridional extent (1.2°, about 134 km). The central westward flow results in an inflow of about 1.3 Sv but experiences a significant seasonality in both flow magnitude (ranging from 2.0 cm/s in summer to 1.4 cm/s in winter) and meridional width (ranging from 125 km in summer to 90 km in winter). In summer, the northern outflow narrows slightly in width with reduced velocities (about 1.0 cm/s), while the central inflow expands northward with increased velocities surpassing the northern outflow; nonetheless, the southern outflow in summer significantly increases and hence still maintains an overall outflow. To sum up, the eastward transport in the intermediate layer of the northern LS exceeds the westward transport in the central LS except in summer, during which time both the central inflow and southern outflow increase, and collectively maintain an outflow in the intermediate layer of the LS.

The intermediate layer of the LS is also marked by distinct vertical variations in circulation patterns, which can be primarily divided into two layers: the upper (412–1000 m) and the lower (1000–1252 m) parts. We examine the horizontal distribution of flow fields at 500 m and 1250 m as the representative currents in the upper and lower intermediate layers, respectively. In the upper intermediate layer (Fig. 6a-c), the annual mean currents not only exhibit a large anticyclonic eddy southwest of Taiwan Island, but also a prominent anticyclonic Kuroshio loop within the LS, flowing northwestward in the central LS and then turning northeastward in the northern outflow segment. While seasonal differences in the overall flow patterns are minor, the flow magnitudes of both the Kuroshio loop and the anticyclone are notably larger in January than in July. The Kuroshio loop embraces a weak anticyclonic structure within the LS, guiding the water from the northern outflow back into the central segment of the strait, which is consistent with the finding of Xie et al. (2011). In the lower intermediate layer (Fig. 6d-f), the seasonal differences in current fields are more pronounced than those in the upper intermediate layer. In January, both the northern outflow and the central inflow areas shift southward compared to their 500-m counterparts (Fig. 6e). The anticyclone southwest of the Taiwan Island is smaller in size and weaker in strength than that at 500 m. To the south of this anticyclone, a stronger anticyclone appears northwest of the Luzon Island, accompanied by a prominent

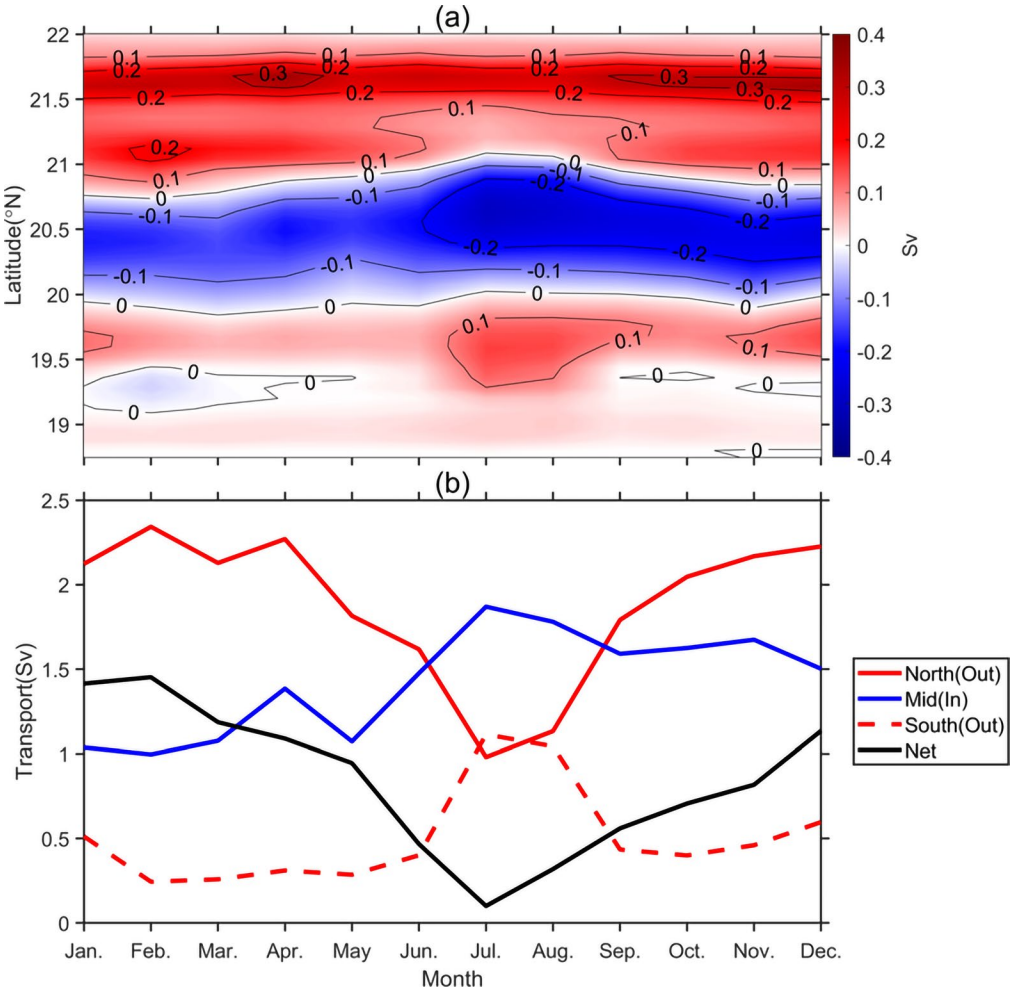

Fig. 5 Seasonal variations of the zonal transport (**a**) along the 121°E section, and (**b**) meridionally integrated over three segments (see details in the main texts), at the intermediate layer (from 412 m to 1252 m) in the LS. Note that the positive values in (**b**) indicate eastward transport in both the northern and southern segments, while representing westward transport in the central segment

eastward flow at 20°N. In July, however, both of these two anticyclonic eddies are absent, and the transport shifts to a predominantly westward inflow in the northern LS.

3.3 The pathways of the intermediate-layer water transport in the Luzon Strait

We now conduct Lagrangian particle tracking experiments to further investigate the pathways of the intermediate-layer water transport in the LS. Specifically, we release particles along the 121°E section at the two representative depths of 500 m and 1250 m to study their trajectories. The above analysis demonstrates the presence of the northern outflow and central inflow in the intermediate layer of LS; therefore, in addition to regular particles that escape from the 121°E section after being released, we will also pay close attention to particles that, after being released, re-enter this section and term this phenomenon as *reflux*. To more accurately isolate the reflux transport, we examine the trajectories of particles released in both the outflow and inflow segments separately. Note that the specific ranges of the outflow and inflow segments vary at different depths.

At 500 m depth, the northern outflow segment spans from 20.6°N to 22°N, within which 68% of the released particles move eastward, accounting for 71% of the total transport in this segment (the transport is related to the velocities of particles). Among these particles, 95% of them (corresponding to 96% eastward transport) flow northeastward into the western Pacific Ocean (Fig. 7a), but a minor fraction (5%) of these particles return to the LS or even to the northern SCS (Fig. 7b). This means that at 500 m depth, particles in the northern outflow segment exhibit reflux, although the transport associated with this reflux is small (4% of total eastward transport). There are primarily two routes for these refluxed particles: (i) a northern route, where 35% of total northern reflux particles moves westward near the release

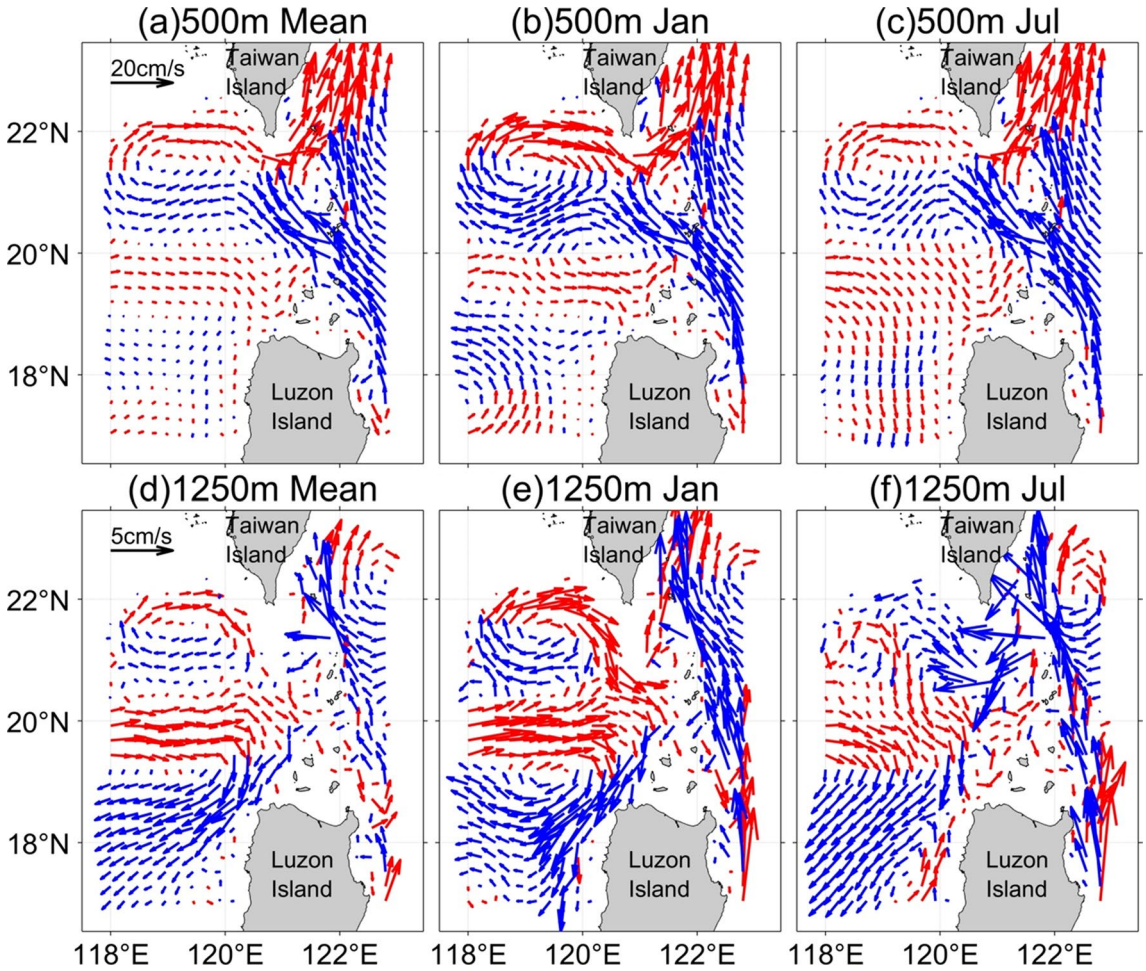

Fig. 6 The flow patterns at 500 m depth for (**a**) annual mean, (**b**) January mean, (**c**) July mean. (**d**), (**e**) and (**f**) are the same as (**a**), (**b**) and (**c**) but at 1250 m depth. The red arrows indicate eastward flow and blue arrows indicate westward flow

location in the northern part of the section, and (ii) a southern route, where 65% of total northern reflux particles return to the section in the central-southern part. Temporally, 26% of the refluxed particles return to the 121°E section within 10 days (1% of total eastward transport), and 89% of the particles return within 60 days (3% of total eastward transport). Some particles have a longer return time, but they remain staying west of 121.5°E instead of excursing far away. For particles released in the central inflow segment (spanning from 19.6°N to 20.6°N), 68% of the particles move westward after released, corresponding to 79% of the total westward transport. Approximately 71% of the westward-moving particles (corresponding to 63% transport) return to the 121°E section (Fig. 7d). The remaining 29% particles directly entering the SCS primarily originate from areas with strong westward currents (corresponding to 37% transport), with the majority moving westward into the northern SCS and a smaller portion moving southward along the Luzon Island into the SCS (Fig. 7c). Therefore, the reflux in the upper intermediate layer in the LS is primarily manifested between the central inflow and northern outflow segments, due largely to the presence of the Kuroshio intrusion and the anticyclonic eddy existed in the LS.

At the depth of 1250 m, the particle trajectories differ significantly from those at 500 m. It should be noticed that the northern outflow segment and the central inflow segment experience southward displacement as a consequence of topographical modifications. In the northern outflow segment (spans from 20°N to 21°N), 54% of the particles move eastward after being released, accounting for 56% of the eastward transport. Among these particles, only 32% of them are directly transported to the western Pacific Ocean, representing 40% of the total northern outflow transport. Their trajectories include not only the northeastward movement along the southeastern coast of the Taiwan Island, but also a considerable number moving directly eastward or southeastward into the western Pacific Ocean (Fig. 8a). The proportion of the refluxed particles and the corresponding transport are significantly higher at 1250 m than those at 500 m, with the majority of these particles moving

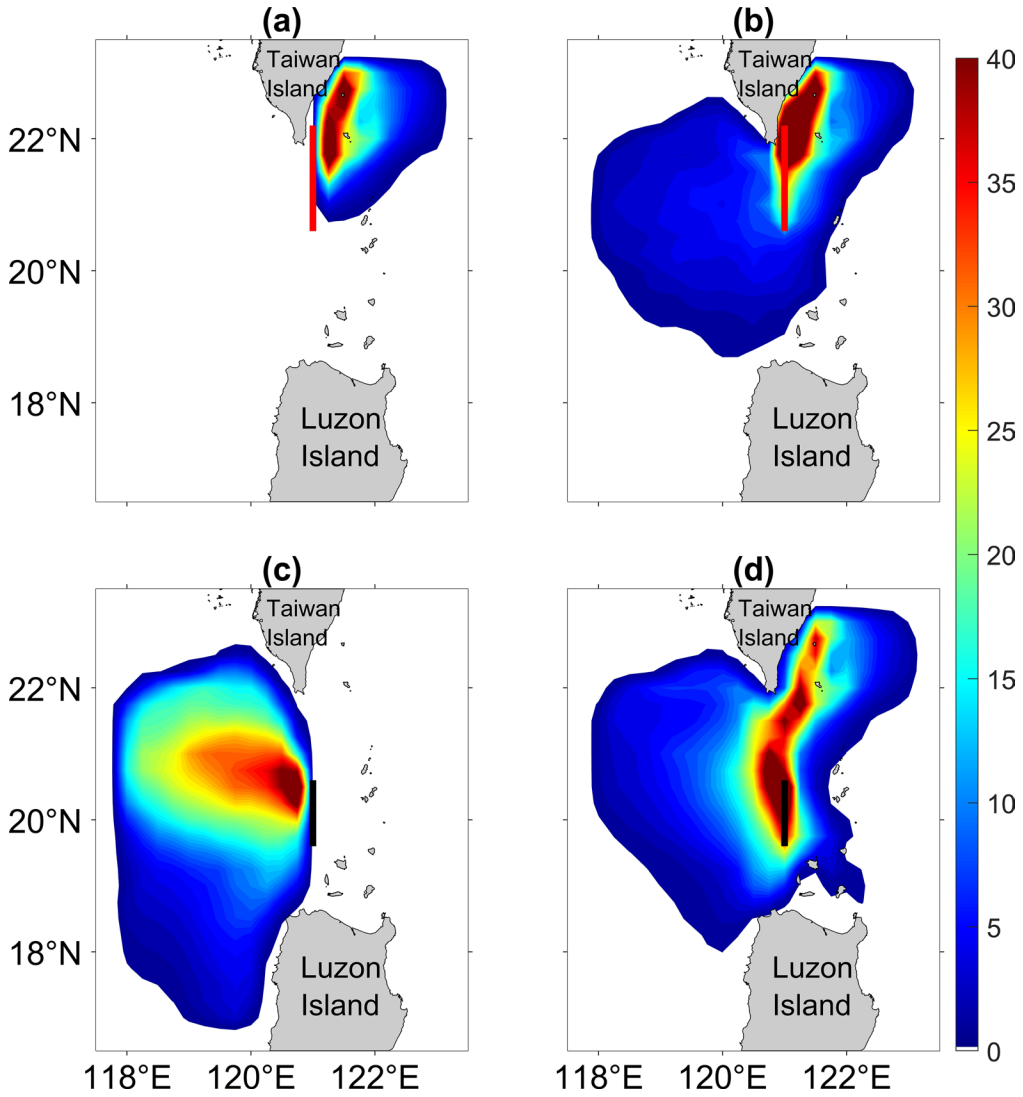

Fig. 7 The trajectory probability of particles released at the 500 m. The red lines indicate the releasing positions in the northern outflow segment for particles initially moving eastward (**a**) without and (**b**) with particles returned to the 121°E section. The black lines represent the releasing positions in the central inflow segment for particles initially moving westward (**c**) without and (**b**) with particles returned to the 121°E section

southwestward into the SCS, and only a few moving northwestwards into the northern SCS (Fig. 8b). Relative to all the refluxed particles, the percentages returning to the section within 10 days, 30 days, and 60 days are 4%, 30%, and 58%, respectively. And the percentages of their corresponding transports relative to total eastward transport are 3%, 18% and 35%, respectively. This indicates that at lower depths, particles in the northern outflow segment are more prone to reflux, although a longer time is required due to the weaker currents at lower depths and the tendency to move southward for the outflow particles. For particles in the central inflow segment (spans from 19°N to 20°N), 55% of particles move westward after being released, corresponding to 59% of the westward transport. Among these particles, 55% of them enter the SCS directly (Fig. 8c), accounting for 71% of the transport. The transport associated with the reflux is relatively small, and the majority of the refluxed particles returns to the SCS again instead of entering the western Pacific Ocean (Fig. 8d). Among the refluxed particles, the percentages returning to the section within 10 days, 30 days, and 60 days are 44%, 63%, and 76%, respectively. And the percentages of their corresponding transport relative to total westward transport are 13%, 19%, and 24%, respectively. The relatively high percentage within 10 days indicates a higher relux efficiency in the central inflow segment compared to that in the northern outflow segment.

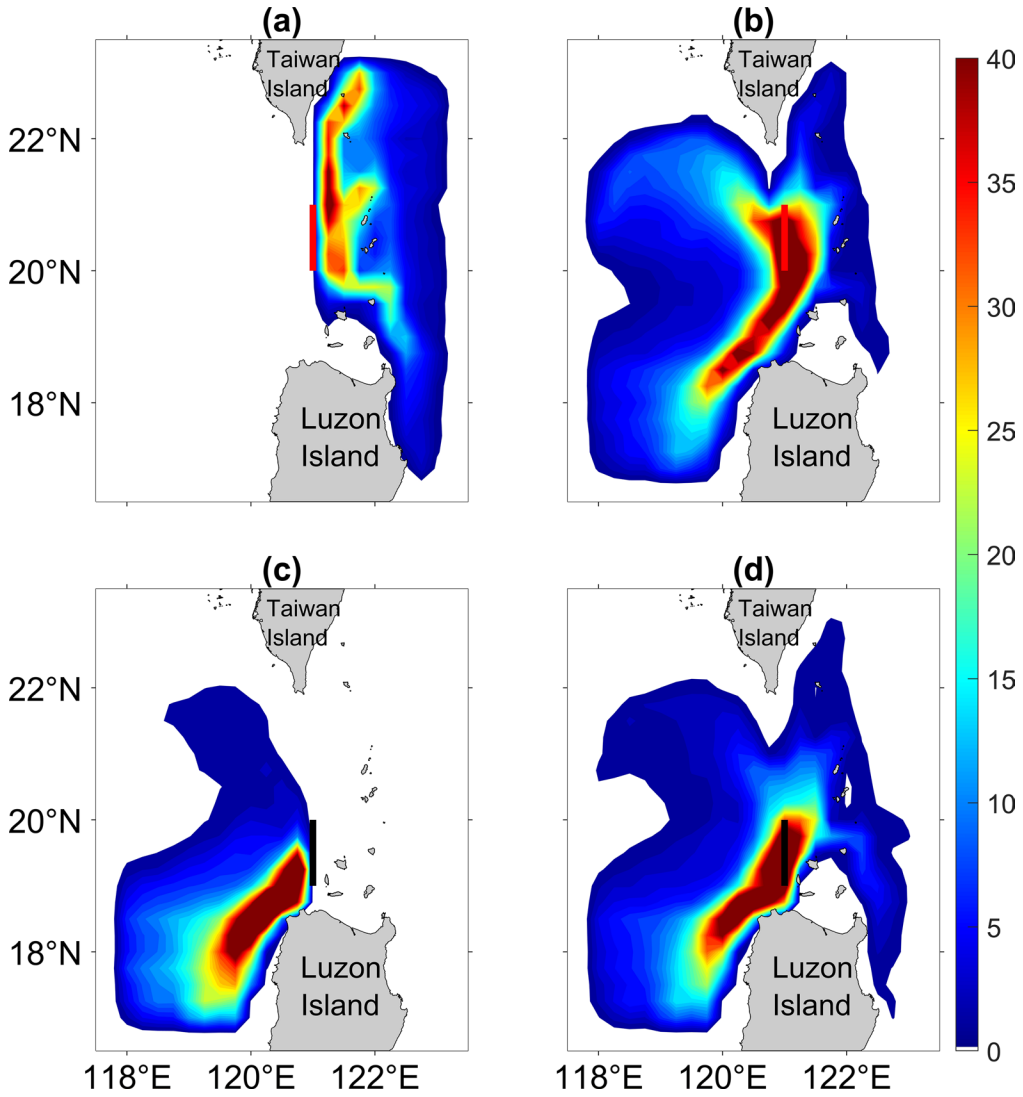

Fig. 8 Same as Fig. 3, but at 1250 m depth

4 Discussions

The Lagrangian particle tracking results reveal that reflux in the intermediate layer of the LS significantly affects the inflow and outflow transports across the strait. This reflux can lead to the western Pacific Ocean water and the SCS water staying in the LS for a longer period of time, thereby weakening the water exchange between the SCS and the Pacific Ocean. The main manifestations of reflux in the intermediate layer can be divided into two cases in terms of particle trajectories: one is the direct return of particles to the 121°E section shortly after release, and the other group of particles has a longer period of excursions on both sides of the section before returning. The reflux for the first case presumably involves higher-frequency flow changes in the LS, whereas for the second case, the reflux is likely associated with lower-frequency variability of the flows outside the LS. Both cases occur at different depths but differ in pattern and quantity. At 500 m, particles exiting from the northern outflow segment rarely returns to the central inflow segment, and even when the reflux occurs, most particles eventually enter the Pacific Ocean (Fig. 7b). With regard to the timescale, the reflux particles in the northern outflow segment can cover the area between 120°E and 122°E within a 10-day period (Fig. 9), and most reflux particles will return to the section within 60 days after being released. At 500 m, since particles move faster, more reflux particles belong to the first case (shorter-term reflux) than to the second case; for the second case, particles typically move toward the northeastern side of the section before returning (Fig. 9a). At 1250 m, the number of reflux particles from the northern outflow is higher than that at 500 m, namely more reflux particles belong to the second case. Also, most reflux particles at this depth enter the SCS (Fig. 8d) with a slower

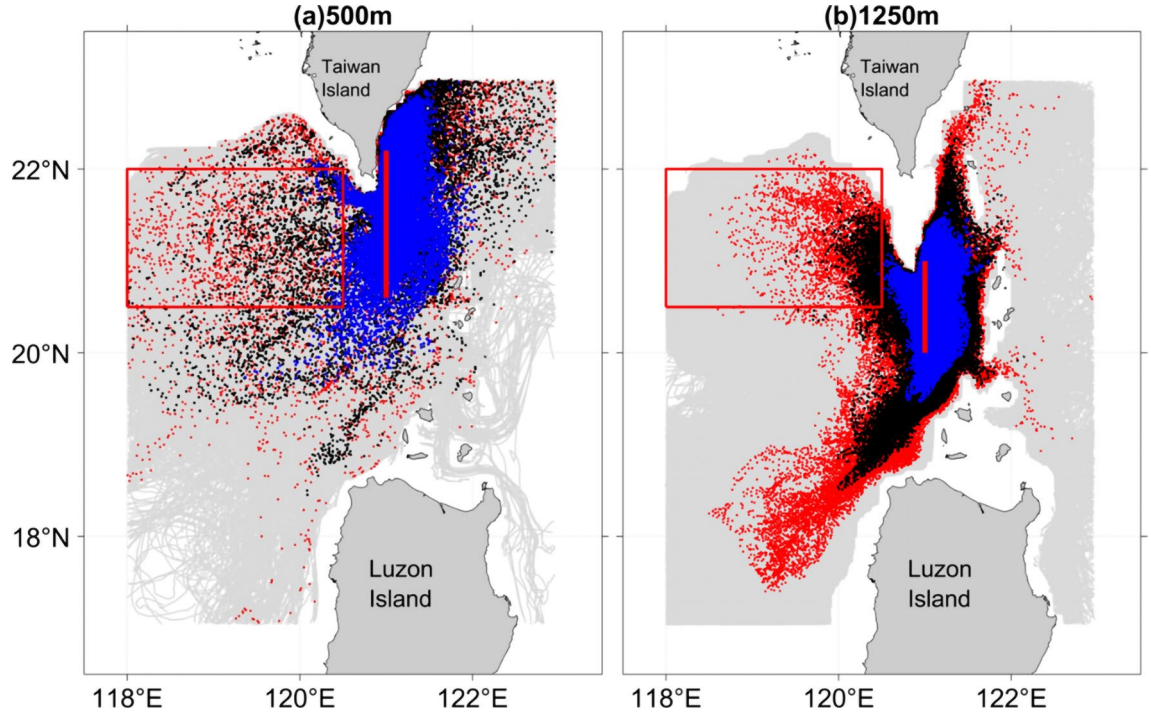

Fig. 9 Trajectories (gray lines) of particles released at the depths of (**a**) 500 m and (**b**) 1250 m in the northern segment. Blue, black and red dots indicate particle positions at 10, 30, and 60 days after being released, respectively. The rectangular area enclosed by the red lines represents the eddy region

movement speed (see red dots in Fig. 9b). At both the 500 m and 1250 m levels, a portion of the reflux particle tracks in the northern outflow segment (approximately 20% of the total northern reflux particles at 500 m and 31% at 1250 m) enter the region southwest of Taiwan Island (indicated by the red rectangular area in Fig. 9), suggesting that the anticyclonic eddy in this region may significantly modulate the reflux in the northern segment.

In terms of the temporal variability of the reflux, the number of reflux particles from the northern outflow segment at 500-m depth shows significant interannual variability, with 1996 and 2012 exhibiting much higher proportions than other years (Fig. 10a, solid red line). Notably, the proportion of the northern reflux particles in 2012 exceeds 10% (a majority of them occurred in November and December), whereas in 2005 the proportion is less than 3%. The high value in 2012 may be related to an anomalous southern flow in the eastern LS (Fig. 11), providing conducive conditions for particles to move southward and to reflux. Reflux via the central inflow segment at 500 m exhibits mild interannual variability, with the proportion of reflux particles ranging between 4% and 6%. Seasonal variation shows that the 500-m reflux in the northern segment occurs more in winter than that in other seasons (Fig. 10b), likely due to the existence of the anticyclone within the LS in winter. Reflux in the central segment at this depth shows weaker seasonal variability and looks relatively higher in spring and October. At 1250 m, the interannual variability of reflux is less prominent than at that 500 m; this is true for both the northern outflow and central inflow segments (Fig. 10a, dashed lines). By contrast, the seasonal variability of reflux at 1250 m is more evident than at 500 m. Reflux in the northern segment is relatively high from late winter to spring, while in the central segment, reflux at this depth is evidently higher in May and June (Fig. 10b, dashed lines).

5 Conclusions

This study investigates the pathways of transport and reflux at different depths in the intermediate layer of the LS, based on analyses of particle trajectories released at the 121°E section using 20 years of high-resolution HYCOM reanalysis data. According to the direction of zonal transports, the intermediate layer can be meridionally divided into three segments, and here we primarily focus on the northern outflow and central inflow segments, and their respective connections with the reflux. The majority of reflux occurs within 60 days starting from the releasing of particles and can be generally categorized into two cases: the first case involves particles returning to the 121°E section shortly after being released, and the second case involves particles moving and staying for a longer period of time on both sides

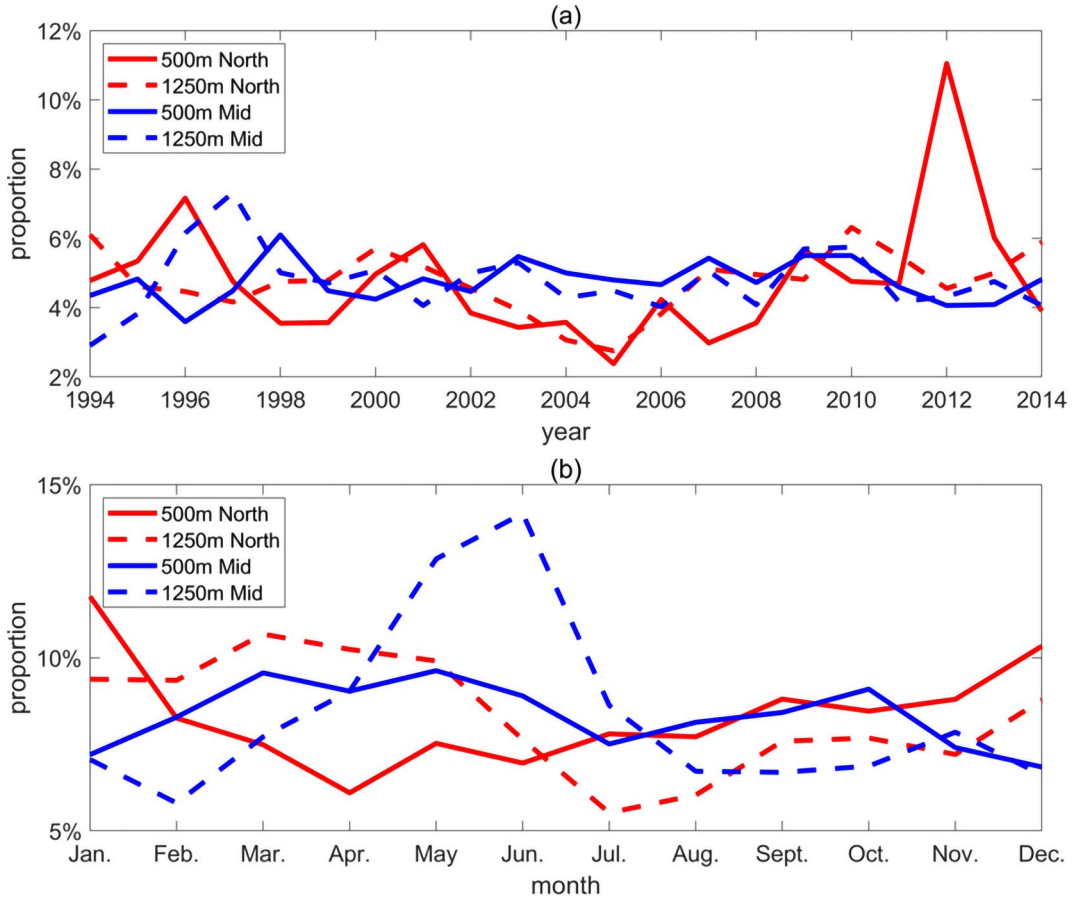

Fig. 10 (**a**) Interannual and (**b**) seasonal variations of the proportions of reflux particles released from the northern segment (red lines) and central segment (blue lines) at the depths of 500 m (solid lines) and 1250 m (dashed lines)

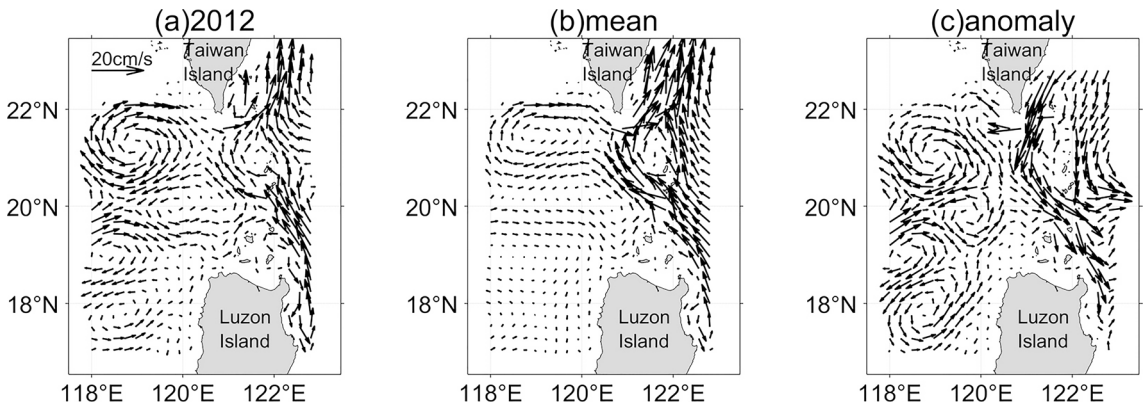

Fig. 11 The mean flow patterns at 500 m depth for (**a**) the year 2012 and (**b**) the entire study period. Panel (**c**) shows the difference between the two flow fields, i.e., (**a**) minus (**b**)

of the strait, facilitating communications between the northern outflow and central inflow segments.

There are significant differences in the zonal transport and reflux at different depths of the intermediate layer due to varying flow fields. At the 500 m depth, reflux is predominantly associated with the central inflow segment. A large number of particles released in the central segment follow the Kuroshio intrusion path into the northern segment and then return to the Pacific Ocean. In contrast, only a small number of particles released in the northern outflow segment return to the southern segment of the strait; most of these particles enter the Pacific Ocean along the southeastern coast of Taiwan Island, accounting for a primary source of SCS water transport into the Pacific Ocean. There is more

reflux of the northern outflow in winter than in summer, primarily due to the presence of a relatively strong anticyclone within the LS in winter. At 1250 m depth, the northern outflow is more prone to reflux, with a proportion exceeding 50%. As for the central segment, the reflux transport is relatively smaller than that at the 500 m depth, and most reflux particles finally return to the SCS rather than to flow into the Pacific Ocean. Although the overall transport in the intermediate layer shows an outflow from the SCS to the western Pacific Ocean, a large amount of water does not enter the western Pacific Ocean due to strong reflux, which makes the water return to the SCS or remain in the LS.

This study explores the pattern, contribution, and seasonal variation of the intermediate layer reflux in the LS based on long-term reanalysis data, but the mechanisms causing the interannual variability of reflux remain to be studied. Additionally, the interplay between the intermediate layer and the other layers, and the roles of such interplay on the reflux might worth exploring in the next step.

Acknowledgements The authors thank the two anonymous reviewers for their constructive comments.

Author contributions W.Z. and J.H. developed the initial concept. Z.Y. analyzed the data and prepared all figures. Z.Y. and H.L. wrote the main manuscript text. All authors contributed to reviewing and revising the manuscript.

Funding This study is supported by the National Natural Science Foundation of China (91958203), the Natural Science Foundation of Fujian Province of China (2023J01021), the International Partnership Program of Chinese Academy of Sciences (059GJHZ2023104MI).

Data availability HYCOM + NCODA GOFS 3.1 global reanalysis data used in this study can be downloaded from https://www.hycom.org/dataserver/gofs-3pt1/reanalysis.

Declarations

Competing interests The authors declare no competing interests.

References

Aoki S, Imawaki S (1996) Eddy activities of the surface layer in the western North Pacific detected by satellite altimeter and radiometer. J Oceanogr 52:457–474. https://doi.org/10.1007/bf02239049

Cai Z, Gan J, Liu Z et al (2020) Progress on the formation dynamics of the layered circulation in the South China Sea. Prog Oceanogr 181:102246. https://doi.org/10.1016/j.pocean.2019.102246

Chen G, Hu P, Hou Y, Chu X (2011) Intrusion of the Kuroshio into the South China Sea, in September 2008. J Oceanogr 67:439–448. https://doi.org/10.1007/s10872-011-0047-y

Cummings JA, Smedstad OM (2013) Data Assimilation for Atmospheric, Oceanic and Hydrologic Applications (Vol. II). 303–343. https://doi.org/10.1007/978-3-642-35088-7_13

Gan J, Li H, Curchitser EN, Haidvogel DB (2006) Modeling South China Sea circulation: response to seasonal forcing regimes. J Geophys Res Oceans 111:C06034. https://doi.org/10.1029/2005jc003298

Gan J, Liu Z, Hui CR (2016) A three-layer alternating spinning circulation in the South China Sea. J Phys Oceanogr 46:2309–2315. https://doi.org/10.1175/jpo-d-16-0044.1

Hu J, Zheng Q, Sun Z, Tai C (2012) Penetration of nonlinear rossby eddies into South China Sea evidenced by cruise data. J Geophys Res Oceans 117:C03010. https://doi.org/10.1029/2011jc007525

Jiang Y, Zhang S, Tian J et al (2020) An examination of circulation characteristics in the Luzon Strait and the South China Sea using high-resolution Regional Atmosphere-Ocean coupled models. J Geophys Res Oceans 125(6). https://doi.org/10.1029/2020jc016253. e2020JC016253

Kehl C, Nooteboom PD, Kaandorp MLA, van Sebille E (2023) Efficiently simulating Lagrangian particles in large-scale ocean flows — data structures and their impact on geophysical applications. Comput Geosci 175:105322. https://doi.org/10.1016/j.cageo.2023.105322

Lan J, Zhang N, Wang Y (2013) On the dynamics of the South China Sea deep circulation. J Geophys Res Oceans 118:1206–1210. https://doi.org/10.1002/jgrc.20104

Lan J, Wang Y, Cui F, Zhang N (2015) Seasonal variation in the South China Sea deep circulation. J Geophys Res Oceans 120:1682–1690. https://doi.org/10.1002/2014jc010413

Lange M, van Sebille E (2017) Parcels v0.9: prototyping a Lagrangian ocean analysis framework for the petascale age. Geosci Model Dev 10:4175–4186. https://doi.org/10.5194/gmd-10-4175-2017

Li L, Nowlin WD, Jilan S (1998) Anticyclonic rings from the Kuroshio in the South China Sea. Deep Sea Res Part I: Oceanogr Res Pap 45:1469–1482. https://doi.org/10.1016/s0967-0637(98)00026-0

Nan F, Xue H, Yu F (2015) Kuroshio intrusion into the South China Sea: a review. Prog Oceanogr 137:314–333. https://doi.org/10.1016/j.pocean.2014.05.012

Qu T, Girton JB, Whitehead JA (2006) Deepwater overflow through Luzon Strait. J Geophys Res Oceans 111:C01002. https://doi.org/10.1029/2005jc003139

Shen J, Zhang J, Li L (2022) Deep and intermediate exchange patterns through the Luzon Strait as revealed by synoptic hydrographic observation. Deep Sea Res Part I: Oceanogr Res Pap 181:103705. https://doi.org/10.1016/j.dsr.2022.103705

Shu Y, Xue H, Wang D et al (2014) Meridional overturning circulation in the South China Sea envisioned from the high-resolution global reanalysis data GLBa0.08. J Geophys Res Oceans 119:3012–3028. https://doi.org/10.1002/2013jc009583

Sun Z, Zhang Z, Huang RX et al (2023) Novel insights into the zonal flow and transport in the Luzon Strait based on long-term mooring observations. J Geophys Res Oceans 128(3). https://doi.org/10.1029/2022jc019017. e2022JC019017

Tian J, Yang Q, Liang X et al (2006) Observation of Luzon Strait transport. Geophys Res Lett 33:L19607. https://doi.org/10.1029/2006gl026272

Tian J, Yang Q, Zhao W (2009) Enhanced diapycnal mixing in the South China Sea. J Phys Oceanogr 39:3191–3203. https://doi.org/10.1175/2009jpo3899.1

Trott CB, Metzger EJ, Yu Z (2021) Investigating mesoscale characteristics eddy in the Luzon Strait region using altimetry. Ocean Dynam 71:679–698. https://doi.org/10.1007/s10236-021-01460-1

Wang D, Xiao J, Shu Y et al (2016) Progress on deep circulation and meridional overturning circulation in the South China Sea. Sci China Earth Sci 59:1827–1833. https://doi.org/10.1007/s11430-016-5324-6

Wu J, Lao Q, Chen F et al (2021) Water mass processes between the South China Sea and the western Pacific through the Luzon Strait: insights from hydrogen and oxygen isotopes. J Geophys

Res Oceans 126(8). https://doi.org/10.1029/2021jc017484. e2021JC017484

Xie L, Tian J, Zhang S et al (2011) An anticyclonic eddy in the intermediate layer of the Luzon Strait in Autumn 2005. J Oceanogr 67:37–46. https://doi.org/10.1007/s10872-011-0004-9

Yuan Y, Liao G, Guan W et al (2008) The circulation in the upper and middle layers of the Luzon Strait during spring 2002. J Geophys Res Oceans 113:C06004. https://doi.org/10.1029/2007jc004546

Yuan Y, Liao G, Yang C (2009) A diagnostic calculation of the circulation in the upper and middle layers of the Luzon Strait and the northern South China Sea during March 1992. Dyn Atmos Oceans 47:86–113. https://doi.org/10.1016/j.dynatmoce.2008.10.005

Zhai X, Johnson HL, Marshall DP (2010) Significant sink of ocean-eddy energy near western boundaries. Nat Geosci 3:608–612. https://doi.org/10.1038/ngeo943

Zhang Z, Zhao W, Tian J, Liang X (2013) A mesoscale eddy pair southwest of Taiwan and its influence on deep circulation. J Geophys Res Oceans 118:6479–6494. https://doi.org/10.1002/2013jc008994

Zhang Z, Zhao W, Tian J et al (2015) Spatial structure and temporal variability of the zonal flow in the Luzon Strait. J Geophys Res Oceans 120:759–776. https://doi.org/10.1002/2014jc010308

Zheng Q, Lin H, Meng J, et al (2008) Sub-mesoscale ocean vortex trains in the Luzon Strait. J Geophys Res Oceans 113:C04032. https://doi.org/10.1029/2007jc004362

Zhu Y, Fang G, Wei Z et al (2016) Seasonal variability of the meridional overturning circulation in the South China Sea and its connection with inter-ocean transport based on SODA2.2.4. J Geophys Res Oceans 121:3090–3105. https://doi.org/10.1002/2015jc011443

Publisher's note Springer Nature remains neutral with regard to jurisdictional claims in published maps and institutional affiliations.

Springer Nature or its licensor (e.g. a society or other partner) holds exclusive rights to this article under a publishing agreement with the author(s) or other rightsholder(s); author self-archiving of the accepted manuscript version of this article is solely governed by the terms of such publishing agreement and applicable law.